CDDpress

www.nature.com/cdd

ARTICLE

Check for updates

The embryonic patterning gene *Dbx1* governs the survival of the auditory midbrain via *Tcf7l2-Ap2δ* transcriptional cascade

Hong-Nhung Tran[1], Quy-Hoai Nguyen[1], Ji-eun Jeong[1], Duc-Linh Loi[1], Youn Hee Nam[2], Tong Ho Kang[2], Jaeseung Yoon[1], Kwanghee Baek[1] and Yongsu Jeong[1]✉

At the top of the midbrain is the inferior colliculus (IC), which functions as the major hub for processing auditory information. Despite the functional significance of neurons in the IC, our understanding of their formation is limited. In this study, we identify the embryonic patterning gene *Dbx1* as a key molecular player that governs genetic programs for IC survival. We find that *Dbx1* plays a critical role in preventing apoptotic cell death in postnatal IC by transcriptionally repressing *c-Jun* and pro-apoptotic BH3 only factors. Furthermore, by employing combined approaches, we uncover that *Tcf7l2* functions downstream of *Dbx1*. Loss of *Tcf7l2* function causes IC phenotypes with striking similarity to those of *Dbx1* mutant mice, which include defective embryonic maturation and postnatal deletion of the IC. Finally, we demonstrate that the *Dbx1-Tcf7l2* cascade functions upstream of *Ap-2δ*, which is essential for IC development and survival. Together, these results unravel a novel molecular mechanism for IC maintenance, which is indispensable for normal brain development.

Cell Death & Differentiation (2023) 30:1563–1574; https://doi.org/10.1038/s41418-023-01165-6

INTRODUCTION

The auditory midbrain or inferior colliculus (IC) is the major hub serving as a critical integration center of the central auditory pathway [1]. To process the perception of sound stimuli, neurons in the auditory system form precise circuits, which emerge from cochlea ganglion neurons. The IC receives virtually all ascending brainstem inputs and descending projection from the auditory cortex [2, 3]. In turn, the IC projects to the medial geniculate body, the thalamic relay nucleus [4, 5]. Neurons in the IC also receive many non-auditory inputs from the superior colliculus (SC), which is known as the optic midbrain. The IC is functionally subdivided into core (central nucleus) and shell (dorsal and lateral cortex) subregions according to dendritic morphology and axonal trajectories [1]. Despite the functional significance of IC neurons, our understanding of their formation is limited.

During early embryogenesis, the territories of midbrain progenitors are specified and assigned into seven subdivisions (m1-m7) with specific combinations of gene expression codes [6, 7]. The m1-m2 regions are organized into the dorsal midbrain or tectum, which further subdivide into the IC and SC. Early growth and patterning of the tectum are tightly linked to the key signaling molecules of the isthmic organizer [8–11]. FGF signaling functions in a dose- and time- dependent manner to control tectal growth, specification, and survival [10, 12, 13]. Distinct levels of FGF activity play crucial roles in regulating SC and IC fates, as reduced FGF signaling results in disruption of the IC [10, 12, 14–16]. In addition, inactivating Fgf8 at different stages leads to variable truncation of the developing tectum [17]. Similarly, loss of the tectum has been also observed in embryos that lack Wnt1 or En1 function although the phenotypes of *Wnt1*- or *En1*-deficient embryos with altered midbrain and cerebellum can vary [18–20]. Impaired cellular processes including defective proliferation, cell fate transformation, and loss of tectal stem zone are likely to be responsible for the loss of the tectum [12, 13, 17]. Furthermore, abnormal apoptosis also appears to be one of the major causes for embryonic tectum deletion [10, 21]. *Pax* and *Meis2* play differential roles in forming the tectum [14, 22–24], and *Otx2* contributes to the control of multiple aspects of midbrain development [25–28]. During neurogenesis between E11.5 and E14.5 [29–32], the tectum produces glutamatergic and GABAergic neurons in the SC and IC [6, 7]. The transcription factors *Ascl1*, *Helt*, *Gata2* and *Tal2* play selective functions in determining GABAergic neuronal identity along the DV axis [6, 7, 33–37]. Although previous works have greatly broadened our understanding of the early phase of tectal development, little is known about the molecular mechanisms underlying the differentiation and survival of the IC at the late embryonic and adult stages.

Herein we present evidence that the transcriptional cascade of the *Dbx1*, *Tcf7l2* and *Ap-2δ* (*Tfap2d*) transcription factors regulates the survival of the IC. The homeodomain transcription factor *Dbx1* is expressed in various regions of the developing nervous system [38], and is required for regulating neuronal cell fate determination. In the spinal cord, *Dbx1* is necessary for specifying distinct identities of V0 and V1 interneurons that coordinate the alternation of left and right limbs [39–41]. In the hindbrain, *Dbx1* is required for regulating the identity and function of the preBötzinger respiratory neurons [42, 43]. In the forebrain, *Dbx1* is critical for regulating the specification of hypothalamic neurons that control innate behaviors [44]. A recent study by gain- and loss-of-function analyses

[1]Department of Genetics and Biotechnology, College of Life Sciences, Graduate School of Biotechnology, Kyung Hee University, Yongin, Gyeonggi, Republic of Korea. [2]Department of Oriental Medicine Biotechnology, Kyung Hee University, Yongin, Gyeonggi, Republic of Korea. ✉email: yongsu@khu.ac.kr

Received: 16 August 2022 Revised: 3 April 2023 Accepted: 5 April 2023
Published online: 20 April 2023

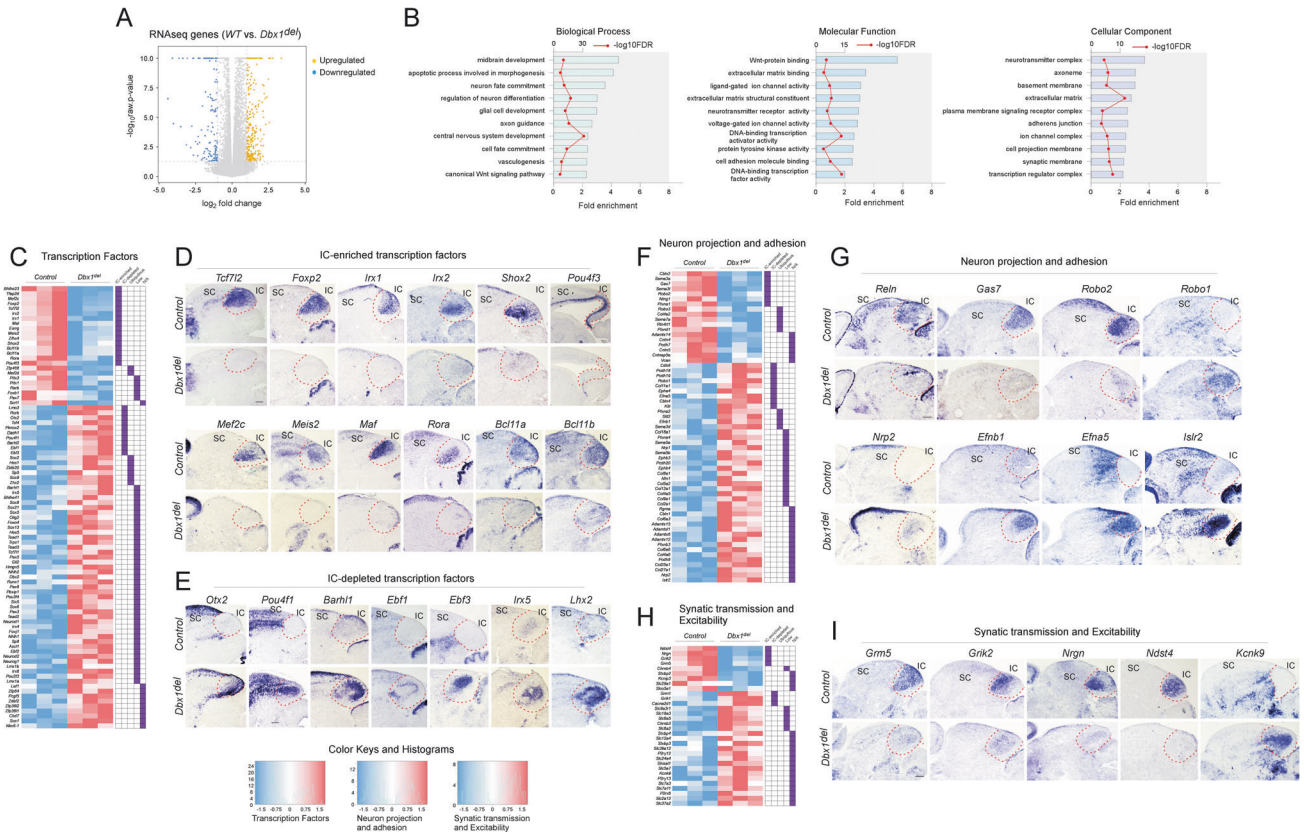

Fig. 1 Differential expression profiling identifies *Dbx1* target genes in the IC. A Volcano plot representing transcriptional changes in $Dbx1^{del}$ IC versus wildtype IC at E18.5. Orange dots correspond to upregulated genes whereas blue dots correspond to downregulated genes. **B** Gene ontology (GO) analysis of differentially expressed genes in the IC of $Dbx1^{del}$ embryos at E18.5 compared with wildtype embryos. Bar charts showing 10 GO terms for biological process, molecular function and cellular components, ranked by fold enrichment. **C**, **F**, **H** Clustering heatmaps represent expression patterns of the genes with overrepresented GO terms: transcription factors (**C**), neuron projection and adhesion (**F**), and synaptic transmission and excitability (**H**). Each column represents an independent biological replicate. The $\log_2$ values of expression in relation to the median of the row are shown as a blue-red color scale. Localization of each gene expression in the brain was estimated according to the Allen Brain Atlas, and is indicated by boxes. IC-enriched, expression enriched in the IC; IC-depleted, expressed broadly in the brain except for the IC; Ubiquitous, expressed throughout the brain; Low, low overall expression in the brain; N/A, not available in the Allen Brain Atlas. **D**, **E**, **G**, **I** In situ hybridization on E18.5 sagittal brain sections. Scale bars, 200 μm.

revealed crucial roles of *Dbx1* in regulating midline crossing by midbrain commissural axons [45]. During early embryogenesis, *Dbx1* expression in the midbrain is restricted to the m1-m2 progenitor domains, which generate IC and SC neurons [28, 38]. At late embryonic stages, *Dbx1* expression is excluded from the SC, and persists in the IC (Allen Brain Atlas). These observations raise the possibility that *Dbx1* has a later role in regulating IC formation. *Tcf7l2*, a high mobility group (HMG) box-containing transcription factor, has been known as both the major transducer of Wnt/β-catenin activity and high diabetic risk factor [46–48]. *Tcf7l2* expression initiates at E10.5, and is abundantly detected in the diencephalon and midbrain [49]. Loss of *Tcf7l2* function leads to pituitary hyperplasia [50], defective oligodendrogenesis [51–53], and disruption of thalamic and habenula development [54–56]. Despite strong and persistent expression in the dorsal midbrain during embryonic and postnatal stages, the possible role of *Tcf7l2* in tectal differentiation remains unexplored.

By employing combined approaches, we demonstrate that *Dbx1-Tcf7l2* transcriptional cascade orchestrates a genetic program for the development of the IC. Notably, this regulatory cascade is required for postnatal survival of the IC by playing an essential anti-apoptotic role through transcriptional suppression of *c-Jun* and BH3-only factors such as *Hrk* and *Bim*. We further show that the *Dbx1-Tcf7l2* cascade acts upstream of *Ap-2δ*, which regulates neuronal survival in the IC [57]. Together, our data begin to define a novel molecular pathway for IC maintenance, which is indispensable for normal brain development.

RESULTS

Dbx1 orchestrates a genetic program for the development of the inferior colliculus

To investigate the role of *Dbx1* in the regulation of IC differentiation, we first generated $Dbx1^{del}$ mice in which *Dbx1* is inactivated at the pre-implantation stages, by crossing $Dbx1^{loxp/loxp}$ mice [44] to *Ella-Cre* [58] transgenic mice. We then analyzed global gene expression in the IC of control and $Dbx1^{del}$ mutant embryos on E18.5 by RNA-seq. In this comparison, we found 1,524 genes differentially expressed (≥0.4 or ≤ −0.4 $\log_2$ fold-change; $P_{adj} <$ 0.05), 1,213 of them upregulated and 311 downregulated in $Dbx1^{del}$ mutants (Fig. 1A; Table S1; Table S2). The differentially expressed genes (DEGs) were significantly enriched in gene ontology (GO) terms associated with transcription factor activity, neuron projection, cell adhesion, synaptic function, apoptotic process, Wnt signaling, ion channel activity, extracellular matrix, and neurotransmitter signaling (Fig. 1B; Table S3). To assess whether the DEGs from these groups are specific to the IC, we surveyed corresponding gene expression data from the Allen Brain Atlas (https://mouse.brain-map.org). We found that 100% of the DEGs highly enriched in the IC belonged to the downregulated target genes (Fig. 1C, F, H).

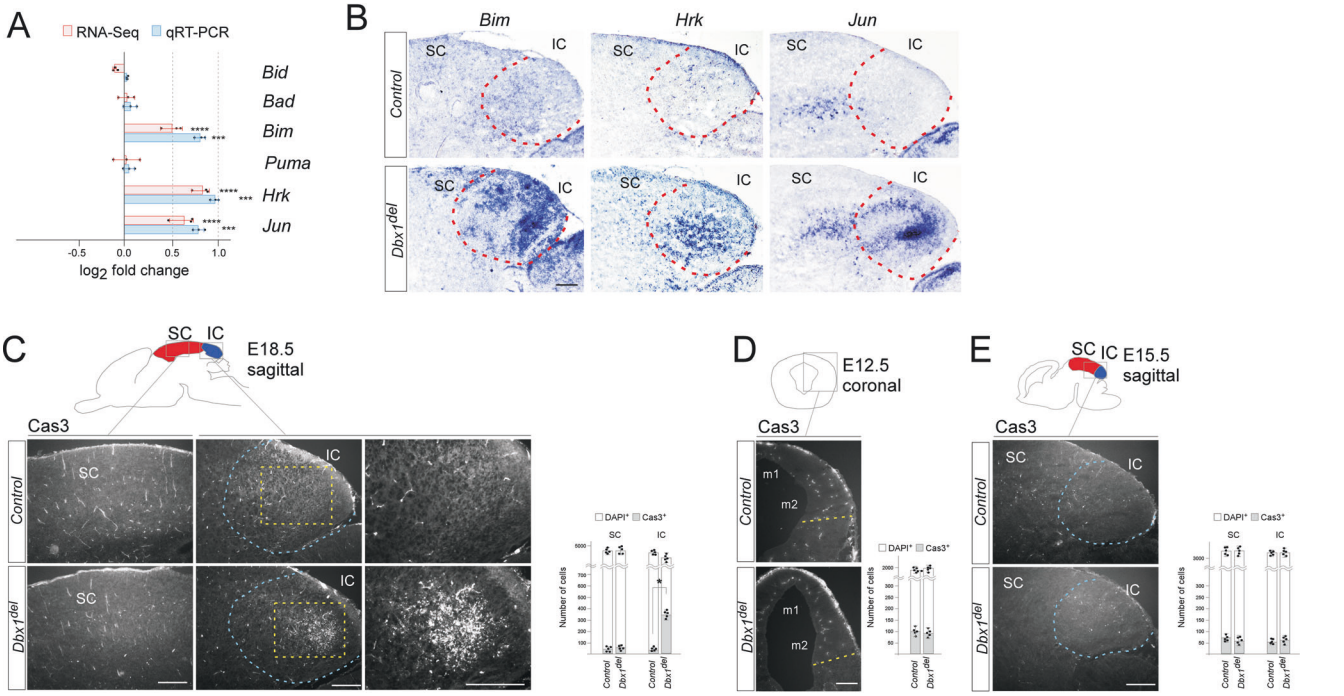

Fig. 2 Loss of *Dbx1* leads to increased levels of c-Jun and BH3 only factors, and to cell death in the IC. A Differential expression of BH3 only (*Bid*, *Bad*, *Bim*, *Puma*, *Hrk*) factors and *c-Jun* in E18.5 $Dbx1^{del}$ compared with control based on RNA-seq (pink bars; ****FDR $q \leq 0.0001$) and qRT-PCR (light blue bars; Student's t-test; ***$p \leq 0.001$); error bars indicate standard error for log2 fold change). **B** In situ hybridization with *Bim*, *Hrk*, and *c-Jun* riboprobes in E18.5 sagittal brain sections. **C**–**E** Immunohistochemistry using anti-cleaved caspase 3 (Cas3) was performed on E18.5 coronal sections (**C**) and E12.5 (**D**) and E15.5 (**E**) sagittal sections to detect apoptosis. E18.5, but not E12.5 or E15.5 $Dbx1^{del}$ mutants exhibited increased numbers of apoptotic cells in the IC. For E12.5, $Cas3^{+}$ cells were counted from 5 sections from each embryo ($n = 5$). For counting $Cas3^{+}$ cells at E15.5 and E18.5, 10–20 counting sites (counting grid for SC, 200 μm × 200 μm; for IC, 100 μm × 100 μm) were evaluated in one section. The values were calculated from 5 sections from each embryo ($n = 5$). *$P < 0.01$ (Student's *t*-test). Scale bars, 200 μm.

To validate this loss of *Dbx1*-altered gene expression in the IC, we selected a subset of the identified DEGs for further analysis by in situ hybridization (ISH). IC-enriched genes included transcription factors *Tcf7l2*, *Foxp2*, *Irx1/2*, *Shox2*, *Pou4f3*, *Mef2c*, *Meis2*, *Maf*, *Rora*, and *Bcl11a/b*; neuronal adhesion *Reln* [59]; axon projection *Gas7* and *Robo2* [45, 60]; synaptic transmission *Grm5*, *Grik2*, *Nrgn*, *Kcnk9* and *Ndst4* [61] (Figs. 1D, G, I, S1A, B). By contrast, the DEGs that were upregulated in the $Dbx1^{del}$ mutant were dominated by genes that were either depleted from the IC, broadly expressed, or undetectable (Fig. 1C, E, F, G, H, I). Among them were transcription factor *Otx2*, *Pou4f1*, *Barhl1*, *Ebf1/3*, *Irx5/6*, and *Lhx2*; chromatin remodeling factor *Chd7*; axon guidance *Robo1*, *Nrp2*, *Ntn1*, *Efna5*, and *Islr2* [62]; basement membrane *Col4a5* [63]; cell adhesion *Pcdh19* [64] (Fig. 1C, F, H). Taken together, these data identify a set of *Dbx1*-regulated genes with potentially novel roles in late phases of IC development.

The expression of *Tcf7l2* and *Meis2* identified the whole IC except for the ventrolateral region, whereas other IC-enriched genes such as *Nrgn*, *Foxp2*, *Maf*, *Ndst4*, *Pou4f3*, and *Barhl1* could serve as subregion-specific IC markers (Fig. S1A, B). *Foxp2*, *Maf*, and *Ndst4* are expressed along the DV axis, and partially overlapped with the expression of *Nrgn*, which is restricted to the dorsolateral region. The ventromedial region in the IC was subdivided into two different cell populations, $Ndst4^{+}$ $Pou4f3^{-}$ cells and $Ndst4^{-}$ $Pou4f3^{+}$ cells (asterisk in Fig. S1A, B). Therefore, our datasets provided a list of molecular markers that distinguish the IC from the SC and other brain regions, and could selectively identify different neuronal types in the IC.

Loss of *Dbx1* leads to upregulation of BH3 only pro-apoptotic genes and robust neuronal cell death in the IC

Because the RNA profile analysis revealed alterations in the expression of genes involved in apoptotic cell death, we next investigated the potential cellular mechanism of the IC defects in the $Dbx1^{del}$ mutant by determining whether *Dbx1* disruption affects neuronal survival in the IC. Among the BH3 only factors implicated in triggering neuronal apoptosis [65–67], the RNA profile showed upregulation of *Bim* and *Hrk* (Tables S2, S3; Fig. 2A). Also, *c-Jun*, the transcription and phosphorylation of which play critical roles in the regulation of BH3 only factors [67, 68], was also upregulated in *Dbx1*-deficient IC. This effect was further validated by RT-PCR and ISH (Fig. 2A, B). Ectopic expression of *Bim*, *Hrk*, and *c-Jun* was specifically detected in the IC of $Dbx1^{del}$ mutants. To determine whether *Dbx1*- deficient IC neurons undergo cell death, we next performed immunostaining for cleaved caspase 3 (Cas3) in the developing midbrain of controls and $Dbx1^{del}$ mutants. At E18.5, loss of *Dbx1* resulted in ~700% increase in the number of IC neurons undergoing apoptosis, compared with control IC (Fig. 2C). By contrast, in the SC, there was no major difference in apoptotic cell death between controls and $Dbx1^{del}$ mutants (Fig. 2C). To determine the timing of the onset of abnormal cell death, we measured immunoreactivity for active Cas3 at earlier stages. At E12.5 and E15.5, there was no significant difference in the number of $Cas3^{+}$ cells in the developing midbrain between controls and $Dbx1^{del}$ mutants (Fig. 2D, E). Therefore, most of the cell death in the $Dbx1^{del}$ -IC occurred at late embryonic stages. These data indicate that *Dbx1* inactivation leads to specific loss of IC cells.

Postnatal deletion of the IC in the absence of *Dbx1*

We next explored the consequence of *Dbx1*-deficiency on the postnatal development of IC neurons. Null mutation of *Dbx1* causes perinatal lethality due to asphyxia resulting from loss of the core respiratory rhythm generator in the hindbrain preBötC complex [42, 43], which precludes analysis of the long- term consequences on dorsal midbrain development. To overcome this

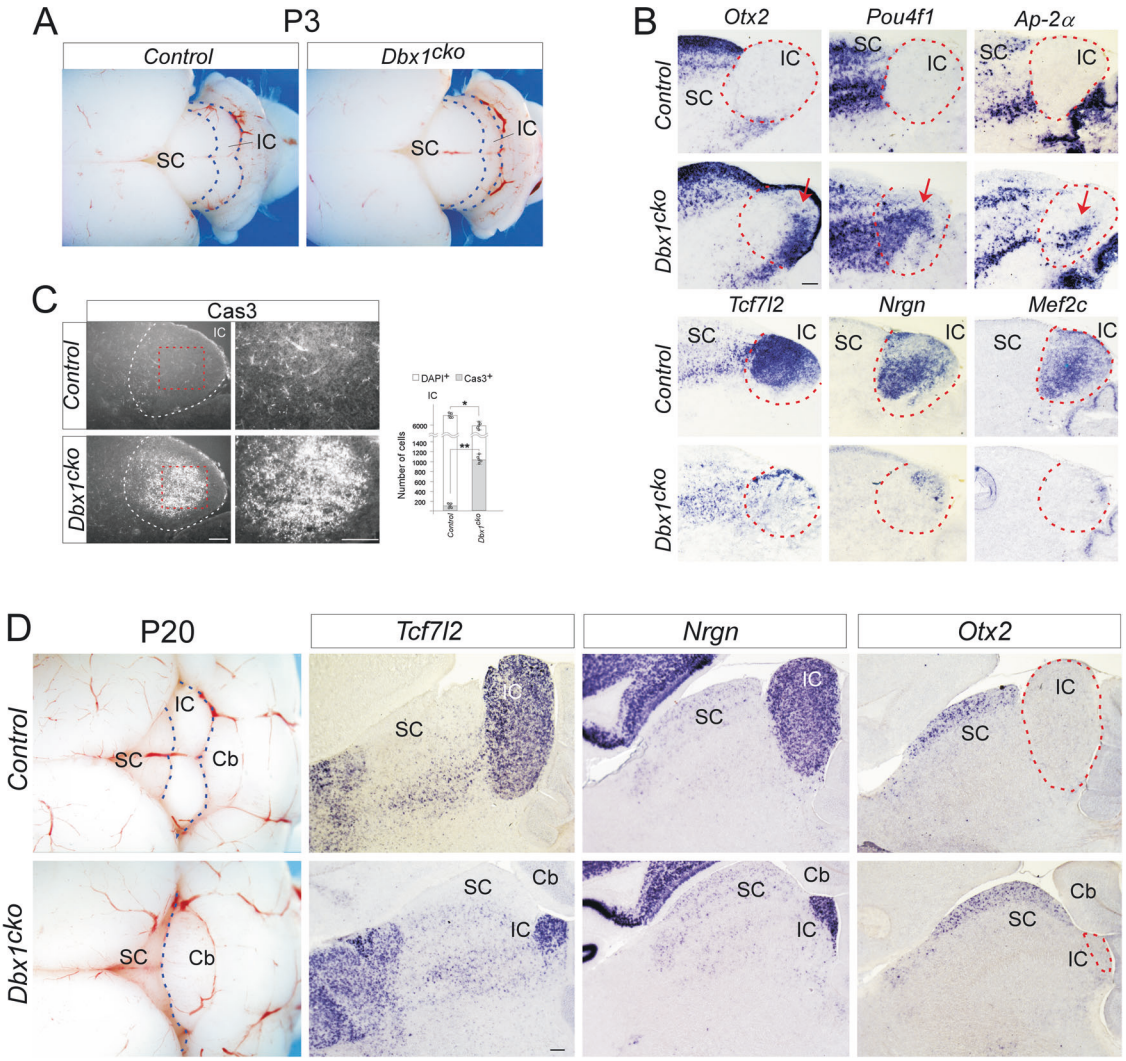

Fig. 3 Absence of the inferior colliculus in *Dbx1^{cko}* mutant mice. A A close-up dorsal view of P3 control and *Dbx1^{cko}* mutant brains. Dashed lines indicate the position of the IC. Compared with controls, *Dbx1^{cko}* mutant brains showed a reduction in IC size. **B** In situ hybridization on P3 sagittal sections of control and *Dbx1^{cko}* brains. **C** Immunohistochemistry with anti-Cas3 on P3 sagittal sections of control and *Dbx1^{cko}* brains. Cas3^{+} cells were counted from five sections from three embryos using 20 counting sites (counting grid 100 μm × 100 μm) in one section. *$P < 0.05$; **$P < 0.001$ (Student's *t*-test). **D** The P20 brain phenotype of *Dbx1^{cko}* mutants. The entire brain (dorsal view) and histological sections of the midbrain. Section ISH on sagittal sections indicates an almost complete lack of the IC with the SC fused to the cerebellum in *Dbx1^{cko}* mutants. Scale bars, 200 μm.

limitation, we generated a mouse line driving Cre- mediated recombination by using a *Sox2* regulatory element (*Sre*), which was shown to direct the transcription of a reporter gene to distinct brain regions except for the hindbrain [69] (Fig. S2A, B). In *Sre-Cre*; *Dbx1$^{loxp/del}$* mice (*Dbx1^{cko}*), *Dbx1* expression was abrogated in the midbrain at E12.5 (Fig. S2C). At P3, when the fissure between the SC and IC is apparent, external anatomical examination of postnatal brains enabled us to identify *Dbx1^{cko}* mice among their littermates. *Dbx1^{cko}* mutant IC was slightly reduced in size, compared with controls, whereas no overt morphological malformations were found in other brain regions (Fig. 3A). Consistent with the *Dbx1^{del}* mutant, the IC in *Dbx1^{cko}* mutants lost expression of *Tcf7l2*, *Nrgn*, and *Mef2c*, but acquired expression of the SC-specific markers *Otx2*, *Pou4f1* and *Ap-2a* (Fig. 3B). Furthermore, the *Dbx1^{cko}* mutants displayed robust apoptotic cell death in the IC (Fig. 3C). By P20, the IC continued to grow and form the two rounded posterior eminences of the quadrigeminal plate in controls, whereas in the absence of *Dbx1*, the IC was almost completely missing, resulting in abutment of the SC on the anterior cerebellum (Fig. 3D). This was corroborated by examination of *Tcf7l2*, *Nrgn* and *Otx2* expressions on sagittal sections (Fig. 3D). These data demonstrate that the embryonic changes mentioned above result in alterations of the postnatal IC, and that *Dbx1* is selectively required for IC neuronal survival by playing an essential anti-apoptotic role.

Transcriptome analyses reveal similar regulatory functions for *Dbx1* and *Tcf7l2*

Among the *Dbx1*-regulated genes that our transcriptome analyses identified, *Tcf7l2* is a good candidate for mediating the function of *Dbx1*, given the temporal and spatial pattern of *Tcf7l2* expression in the developing midbrain. *Dbx1* and *Tcf7l2* transcription in the midbrain was limited to m1-m2 domains, which are organized into the IC and SC. *Dbx1* was expressed in the progenitor region, and *Tcf7l2* in the post-mitotic region (Fig. S3). Early loss of *Dbx1* severely downregulated *Tcf7l2* expression in the IC and SC, whereas later depletion of *Dbx1* abrogated *Tcf7l2* expression in the IC despite normal expression in the SC (Fig. S3), indicating distinct temporal requirements for *Dbx1* in the regulation of *Tcf7l2* transcription.

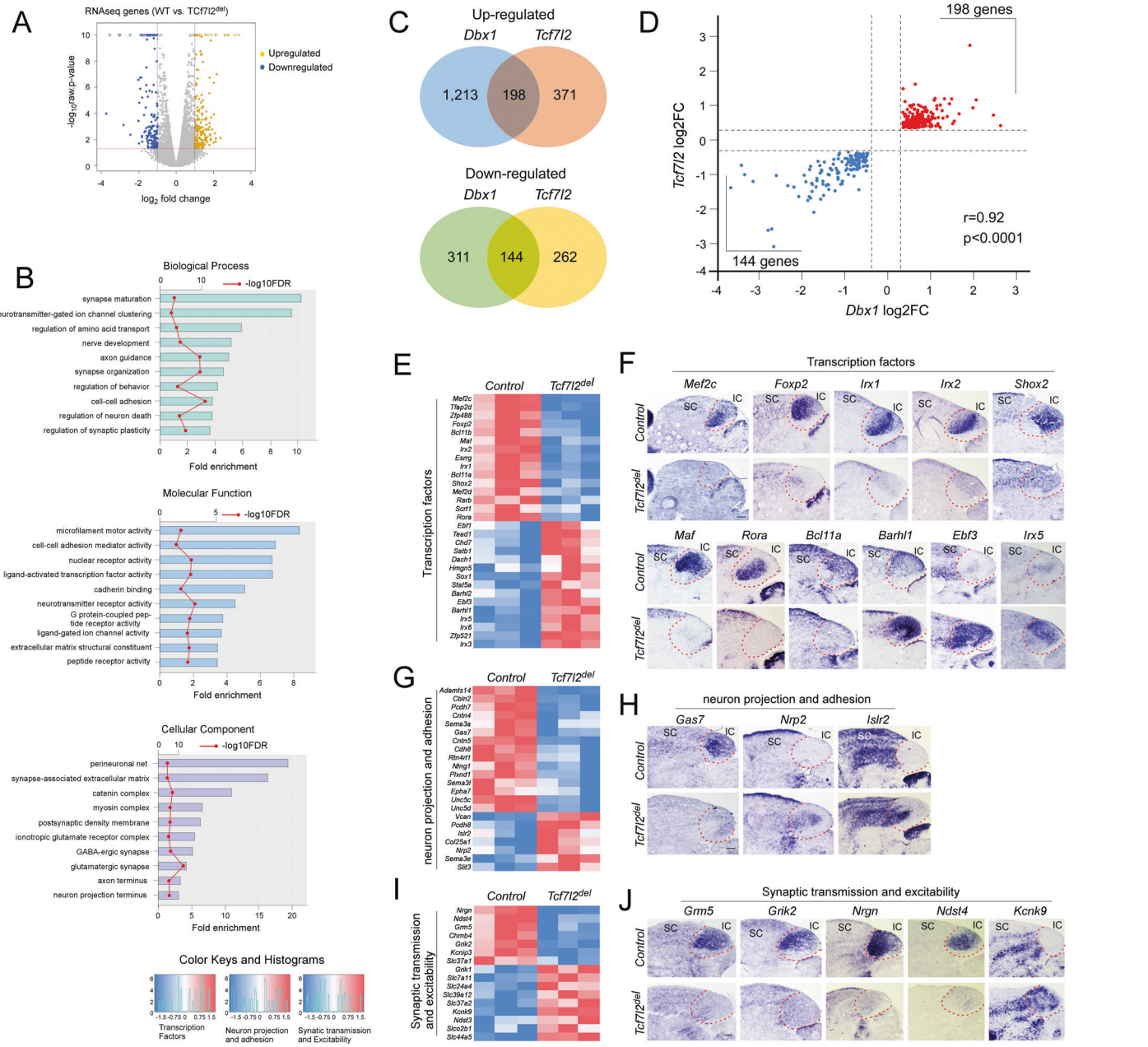

Fig. 4 ***Tcf7l2* acts downstream of *Dbx1* to orchestrate a genetic program of morphological maturation in the developing IC. A** Volcano plot of differential gene expression measured by RNA-seq of wildtype and $Tcf7l2^{del}$ IC. Upregulated or downregulated genes are indicated by orange and blue dots, respectively. **B** GO term enrichment for gene sets that are differentially regulated in $Tcf7l2^{del}$ embryos. Bar charts showing 10 GO terms for biological process, molecular function, and cellular components, ranked by fold enrichment. **C** Intersections of differentially expressed genes in $Dbx1^{del}$ and $Tcf7l2^{del}$ IC identify commonly upregulated and downregulated gene sets. **D** Correlation between the significantly differentially expressed genes ($n = 342$) observed in $Dbx1^{del}$ and $Tcf7l2^{del}$ mutants. Thresholds used to determine differential expression are indicated by dashed lines ($\log_2FC \geq 0.4$ and ≤ -0.4; $P_{adj} \leq 0.05$). The Pearson correlation coefficient is indicated in the lower right corner. **E**, **G**, **I** Clustering heatmap indicating relative expression of the genes with the overrepresented GO terms: transcription factors (**E**), neuron projection and adhesion (**G**), and synaptic transmission and excitability (**I**). Each column represents an independent biological replicate. The $\log_2$ values of expression in relation to the median of the row are shown as a blue-red color scale. **F**, **H**, **J** In situ hybridization on E18.5 sagittal brain sections. Scale bars, 200 μm.

To explore the potential role of *Tcf7l2* in the regulation of tectal development, we generated $Tcf7l2^{del}$ mice by crossing $Tcf7l2^{loxp/loxp}$ mice to the *EIIa-Cre* line, and analyzed transcriptome changes in the IC of control and $Tcf7l2^{del}$ mutant embryos on E18.5 by RNA-Seq. This comparison revealed 633 DEGs (≥0.4 or ≤ −0.4 $\log_2$ fold-change; $P_{adj} < 0.05$), 371 of them upregulated and 262 downregulated in $Tcf7l2^{del}$ mutant (Tables S1, S4, S5; Fig. 4A, B). To identify genes that are co-regulated by *Dbx1* and *Tcf7l2*, we intersected these datasets from $Tcf7l2^{del}$ mutants with our list of *Dbx1*-regulated genes. Out of 633 DEGs that were regulated by *Tcf7l2*, 342 targets (54%; 198 upregulated and 144 downregulated), were commonly affected to a similar extent in $Dbx1^{del}$- and $Tcf7l2^{del}$-mutants (Table S6; Fig. 4C, D). We selected a subset of the common targets to validate their expression in $Tcf7l2^{del}$ mutants by ISH (Fig. 4E–J). Among them were transcription factors *Mef2c*, *Foxp2*, *Irx1/2*, *Shox2*, *Maf*, *Rora*, *Bcl11a*, *Barhl1*, *Ebf3*, and *Irx5*;

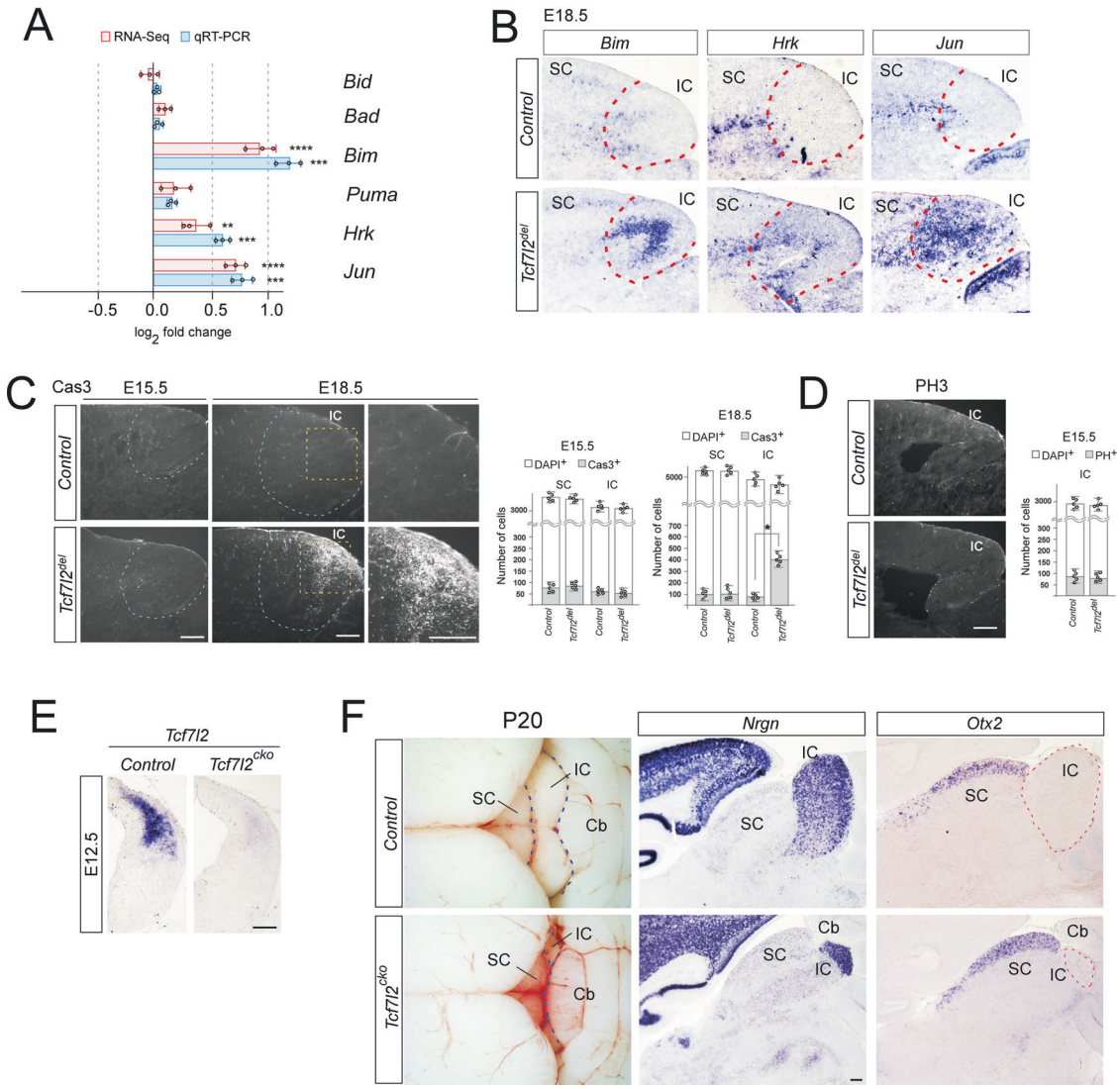

Fig. 5 ***Tcf7l2* inactivation leads to apoptosis and lack of the inferior colliculus. A** Differential expression of BH3-only apoptotic factors and *Jun* in E18.5 *Tcf7l2*^{del} mutants compared with controls based on RNA-seq (pink bars, **FDR $q \leq 0.005$; ****FDR $q \leq 0.0001$) and qRT-PCR (light blue bars, Student's t-test; ***$p \leq 0.001$; error bars indicate standard error for log2 fold change). **B** ISH with *Bim*, *Hrk* and *c-Jun* probe in E18.5 sagittal brain sections. **C** Immunohistochemistry using anti-Cas3 was performed on E15.5 and E18.5 sagittal sections to detect apoptosis. For counting of Cas3^{+} cells at E15.5 and E18.5, 10–20 counting sites (counting grid 100 µm x 100 µm) were evaluated in one section. The values were calculated for five sections from six embryos for each genotype. *$P < 0.001$ (Student's *t*-test). **D** Immunohistochemistry for phospho-histone H3 (PH) on sagittal sections of E15.5 midbrain. The number of PH3-positive cells was counted for three sections from three embryos for each genotype. **E** Section ISH on coronal sections of E12.5 control and *Tcf7l2*^{cko} embryos with a riboprobe derived from exon 10 of *Tcf7l2*. **F** The dorsal view of control and *Tcf7l2*^{cko} mutant P20 brains. Section ISH on sagittal sections indicates large deletion of the IC, whereas the SC abutted on the cerebellum in *Tcf7l2*^{cko} mutants. Scale bars, 200 µm.

neuron projection/adhesion *Gas7*, *Nrp2*, and *Islr2*; synaptic activity *Grm5*, *Grik2*, *Nrgn*, *Ndst4*, and *Kcnk9*. These observations indicate that *Tcf7l2*-deficient IC closely resembles *Dbx1*-depleted IC in its gene expression profile. Taken together, these data suggest that *Tcf7l2* regulates an IC-specific genetic program, and that *Dbx1* and *Tcf7l2* have a significant degree of overlapping regulatory function in the development of the IC.

Deletion of *Tcf7l2* leads to specific loss of the IC due to increased apoptosis

Considering that *Dbx1* and *Tcf7l2* share IC phenotypes through the regulation of common target genes, we asked whether loss of *Tcf7l2* also results in abnormal cell death in the developing midbrain. The RNA profile showed upregulation of *Bim*, *Hrk*, and *Jun* in *Tcf7l2*-deficient IC with a pattern similar to that in *Dbx1*^{del} mutants (Table S4; Fig. 5A). This effect was further confirmed by RT-PCR and ISH (Fig. 5A, B). To determine whether *Tcf7l2* inactivation leads to apoptotic cell death in the developing midbrain, we performed immunostaining for Cas3 in control and *Tcf7l2*^{del} mutant embryos. Loss of *Tcf7l2* resulted in a ~500% increase in the number of Cas3^{+} cells in the IC at E18.5, while control and *Tcf7l2*- deficient SC both had low levels of apoptotic cells (Fig. 5C). We observed no significant differences in the numbers of phospho-histone H3^{+} mitotic cells in the developing midbrain between normal and mutant ICs (Fig. 5D). To further corroborate that prevention of apoptotic cell death by *Tcf7l2* is a critical event during IC development, we examined the effects of *Tcf7l2* on the postnatal development of IC neurons. Because *Tcf7l2*^{del} mutants die shortly after birth due to abnormal intestine development [47, 70], we crossed *Tcf7l2*$^{loxp/loxp}$ mice with a *Sre-Cre* line to bypass perinatal lethality (Fig. 5E). Superficial examination of the brains of *Tcf7l2*^{cko} mutants revealed large deletion of IC with

fusion of the SC to the vermis of the cerebellum (Fig. 5F). Loss of *Tcf7l2* resulted in remarkable reduction in the size of *Nrgn*$^{+}$ domain, while the *Otx2*$^{+}$ SC region was normally detected. Thus, the phenotype of the *Tcf7l2*-depleted IC was essentially the same as that of the *Dbx1*-deficient IC. Taken together, our data indicate that *Tcf7l2* functions downstream of *Dbx1* to regulate survival of the IC.

Ap-2δ is an essential regulator downstream of the *Dbx1-Tcf7l2* cascade

The *AP-2* family of transcription factors plays important roles in regulating cell differentiation and apoptosis [57, 71, 72]. Among the five *AP-2* genes that are expressed in the developing midbrain, only *Ap-2δ* has expression that persists in the IC during embryonic and adult stages. Interestingly, loss of *Ap-2δ* causes massive apoptotic cell death, specifically in the posterior midbrain, and postnatal deletion of the IC [57], resembling the phenotypes of *Dbx1* and *Tcf7l2* mutants. We therefore characterized the transcript levels of *Ap-2δ* in the midbrain in the absence of *Dbx1* or *Tcf7l2*. RNA-seq and qRT-PCR revealed significant reduction in the mRNA expression of *Ap-2δ* in *Dbx1*-deficient or *Tcf7l2*-deficient IC (Fig. 6A; Tables S2, S4, S6). In *Dbx1*^{del} embryos, *Ap-2δ* staining was not detectable in the entire midbrain despite normal expression in other regions during embryogenesis (Fig. 6B). In *Dbx1*^{cko} embryos, *Ap-2δ* expression was largely unaffected in the SC, but abolished in the IC (Fig. 6B). Similarly, loss of *Tcf7l2* did not alter *Ap-2δ* expression in the SC, whereas it severely down-regulated expression in the IC (Fig. 6B). Therefore, our results and

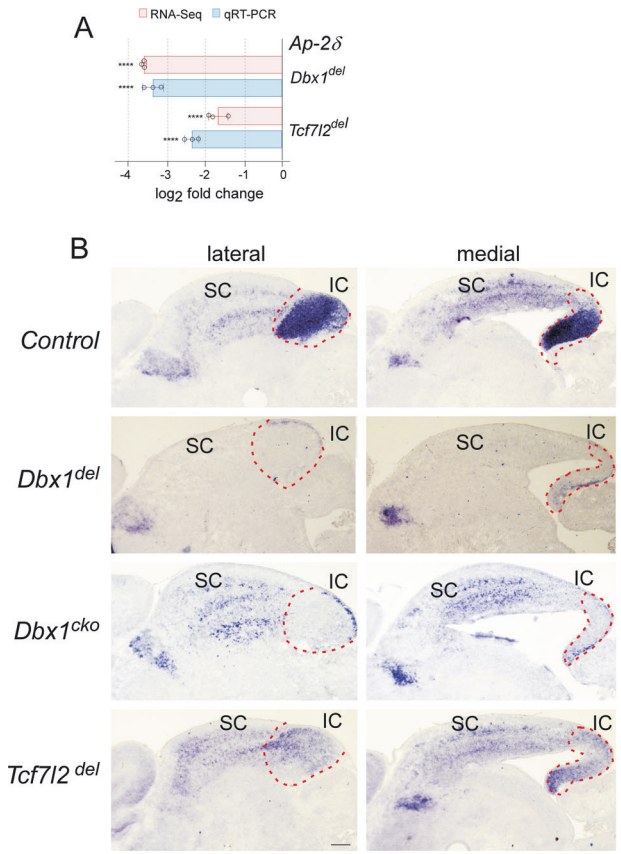

Fig. 6 *Ap-2δ* is co-regulated by *Dbx1* and *Tcf7l2* in the IC. **A** Differential expression of *Ap-2δ* in *Dbx1*^{del} and *Tcf7l2*^{del} mouse embryos compared with controls based on RNA-seq (****FDR $q \leq 0.0001$) and qRT-PCR (Student's t-test; ****$p \leq 0.0001$). Error bars indicate standard error for log2 fold change). **B** Representative midbrain sections of wild-type, *Dbx1*^{del}, *Dbx1*^{cko}, and *Tcf7l2*^{del} mouse embryos hybridized with *Ap-2δ* at E18.5. Scale bars, 200 μm.

those of others suggest that *Ap-2δ* functions downstream of the *Dbx1-Tcf7l2* regulatory axis to control IC morphogenesis by preventing cell death.

Tcf7l2 and *Ap-2δ* are necessary for *Dbx1*-mediated IC survival

The above-described observations led us to ask whether *Tcf7l2* and *Ap-2δ* are essential components of *Dbx1*-mediated genetic programs that support the survival of the IC. To address this question, we established IC cell cultures from E15.5 embryonic brains of control and *Dbx1*^{del} mice. Primary cultures from control IC tissues were found to contain many cells that co-expressed Tcf7l2 and Nrgn immunoreactivity, indicating normal IC cell identity (Fig. 7A). By contrast, consistent with our embryo experiments, the majority of primary cultured *Dbx1*-deficient IC cells were Tcf7l2^{-}, Nrgn^{-} (Fig. 7A). Compared to controls, *Dbx1*^{del} IC cells that had been cultured for 5~7 days in vitro (DIV) showed apoptosis in significantly increased amounts (Fig. 7B). Notably, almost none of Cas3^{+} apoptotic cells expressed Tcf7l2 immunoreactivity (Fig. 7B). When IC cells were allowed to develop for up to 21 DIV, control IC cells were healthy, with round cell bodies and a complex network of neurites (Fig. 7A, C). However, In *Dbx1*-deficient cell cultures, their cell bodies were smaller and shrunken with fragmented neurites (Fig. 7A, C). Some of *Dbx1*^{del} IC cells had begun detaching from the substrate and neurites were not visible. We estimated cell viability during a 28 DIV time course by using Calcein AM, a cell permeable dye, which is converted to fluorescent Calcein in live cells. The number of viable *Dbx1*^{del} IC cells continued to decrease drastically and was <5% by 28 DIV, whereas >50% of control IC cells were viable (Fig. 7D). To address whether restoration of *Tcf7l2* and *Ap-2δ* expression is able to prevent apoptosis and promote survival in *Dbx1*- deficient IC cells, *Tcf7l2* and/or *Ap-2δ* expression constructs were transfected into *Dbx1*^{del} mutant IC cells that had been cultured for 2 DIV together with a GFP expression vector to identify transfected cells. After 7 additional days of culture, GFP-positive cells were evaluated for apoptosis by assessing Cas3 immunoreactivity. The level of apoptosis was significantly decreased in primary cultures of *Dbx1*^{del} IC cells transfected with *Tcf7l2* and/or *Ap-2δ* expression constructs, compared with mock-transfected *Dbx1*^{del} IC cells (Fig. 7E). To determine whether *Dbx1*-deficient IC cells remained viable following transfection, we assessed cell survival using Calcein-AM during a 21 DIV time course. The viability of mock-transfected *Dbx1*^{del} IC cells continued to decrease drastically and was <5% by 21 DIV, whereas >30% of *Dbx1*^{del} IC cells transfected with *Tcf7l2* and/or *Ap-2δ* expression constructs were viable (Fig. 7F), indicating a significant rescue of IC apoptosis by *Dbx1* deficiency. Taken together, these results suggest that *Tcf7l2* and *Ap-2δ* transcription factors are important mediators of *Dbx1* function for IC survival.

DISCUSSION

Previous studies defined core (central nucleus) and shell (dorsal and lateral nucleus) regions of the IC in adult brain mainly by cell size, dendrite morphology, and axonal trajectories according to anterograde or retrograde tracing [2, 73–76]. IC neuronal populations and distributions during embryogenesis remains poorly understood, as assigning subdivisions is not straightforward because of a lack of gene expression profiling. To the best of our knowledge, this is the first study to systematically capture the gene expression profile of the developing IC at the genomic level, and identify an exhaustive list of molecular markers that distinguish the IC from the SC and other brain regions. Some of the IC-enriched genes revealed by our datasets served as molecular markers that could selectively identify different neuronal types in the IC. Most IC cells are *Tcf7l2*$^{+}$ and *Meis2*$^{+}$, and these neuron populations can be further subdivided into several distinct clusters according to differential distributions of other IC-specific genes including *Nrgn*, *Foxp2*, *Maf*, and *Ndst4*

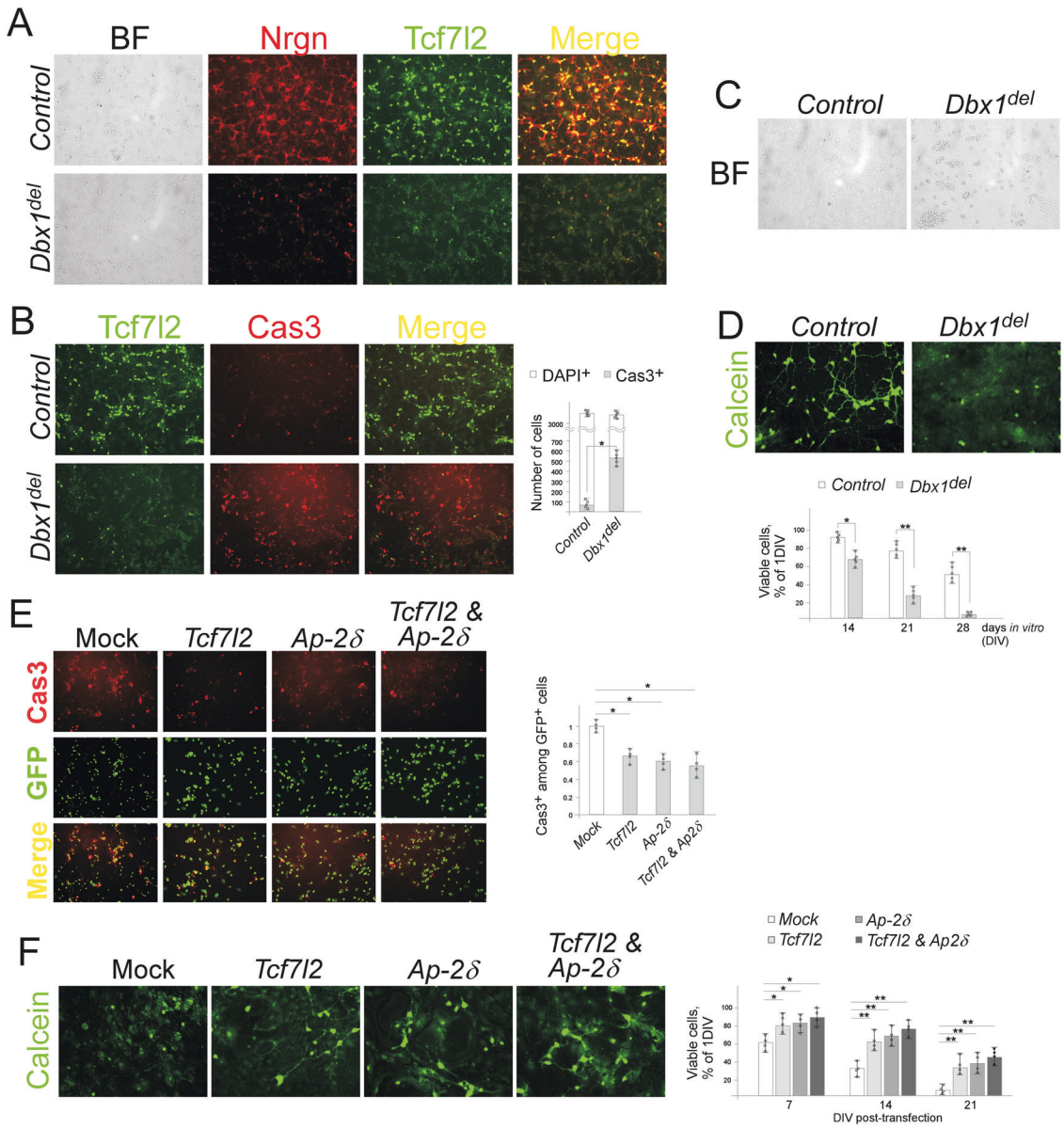

Fig. 7 Restored expression of *Tcf7l2* and/or *Ap-2δ* attenuates apoptosis in *Dbx1*-deficient IC cells. A Isolation and primary cultures of IC cells from E15.5 control and *Dbx1*^{del} mutant embryonic brains. IC cells were cultured on coverslips coated with L-ornithine and laminin in 24-well plates. IC cell identity was verified by immunocytochemistry of 5 days in vitro (DIV5) cells using antibodies against Nrgn and Tcf7l2. Bright-field (BF) images display cellular processes including neurite outgrowth. Consistent with gene expression profiles in embryos, the majority of primary cultured *Dbx1*-deficient IC cells are Tcf7l2^{-}, Nrgn^{-}. **B** Caspase 3 (Cas3) immunostaining were performed at DIV7 cells to identify quantity of apoptosis. Co-immunostaining revealed that most of Cas3^{+} cells are Tcf7l2^{-} ($n = 5$ biological replicates; Student's t-test; *$p \leq 0.001$). **C** Primary IC cells were established from E15.5 embryos and kept in culture for 21 days. Compared to control IC cells with round cell bodies and a complex network of neurites, most of *Dbx1*^{del} mutant cell bodies were smaller, shrunken, and the neurites were fragmented and lost. **D** Calcein AM staining of viable cells. The number of viable cells was determined by Calcein fluorescence at DIV14, DIV21, and DIV28. Six counting sites were evaluated in one coverslip ($n = 5$ biological replicates). *$P < 0.01$; **$P < 0.001$ (Student's *t*-test). **E**, **F** IC cells isolated from *Dbx1*^{del} mutant E15.5 brains were cultured for 2 DIV and transfected with *Tcf7l2* (*p043mTcf-4B*), *Ap-2δ* (*pCMV-Tfap2d*) expression constructs or both DNAs. Nuclear GFP expression construct (*CAG-NLS-GFP*) was co-transfected to identify the transfected cells. **E** Quantification of apoptosis was achieved from IC cells cultured for 7 additional DIV by counting the proportion of Cas3^{+} cells among GFP^{+} cells. Approximately 3000 GFP + cells were considered for each experiments. Histograms represent the means normalized to 1 in the proportion of mock control (empty vector). Experiments were performed in 4 biological replicates. Error bars correspond to standard deviation. Means were compared using Student's t-test; *$p \leq 0.01$). **F** Quantification of survival was achieved from IC cells cultured for 7, 14 and 21 additional DIV following transfection. The number of viable cells was determined by Calcein fluorescence for 6 counting sites in each coverslip (n = 4 biological replicates). (Student's t-test; *$p \leq 0.05$; **$p \leq 0.01$).

(Fig. S1), indicating diverse populations of embryonic IC neurons. Further mapping of the co-expression of more genes in those neuronal clusters at postnatal stages will be required to determine the precise contribution of individual embryonic neuronal subtypes to adult IC organization and connectivity.

Our study shows that *Dbx1* is required for the specification of the progenitor pool in the posterior tectum that generates the *Tcf7l2*$^{+}$ *Meis*$^{+}$ neuronal population in the IC via positive and negative regulation of target genes. It is not surprising that the majority (~80%) of the DEGs are upregulated in *Dbx1* mutants as

Dbx1 functions as a transcriptional repressor that contains the eh1 domain to interact with Gro/TLE corepressor. The downregulated DEGs including *Tcf7l2* and *Meis2*, are likely to be indirectly regulated by *Dbx1*, and other transcriptional repressors released by loss of *Dbx1* may mediate the negative regulation. A question that arises is how this single transcription factor can regulate distinct gene programs along the AP axis of the developing tectum. Our study uncovered striking similarities in IC phenotypes between *Dbx1* and *Tcf7l2* mutants. Interestingly, *Dbx1* is also required for *Tcf7l2* expression in the SC, but unlike the loss of *Dbx1*, loss of *Tcf7l2* did not affect SC differentiation and morphogenesis, indicating that *Dbx1* depends on *Tcf7l2* to promote IC development, and requires other factor(s) for SC differentiation.

Our study uncovered 342 genes that are co-regulated by *Dbx1* and *Tcf7l2*, many of which belong to the list of genes with previously uncharacterized expression and role in the IC, suggesting them as strong candidates for follow-up studies to investigate their functions in IC morphogenesis. Hesse et al. reported the identification of 12 genes, whose expression in the IC is regulated by *Ap-2δ* [57]. Interestingly, five of these *Ap-2δ* targets; *Mef2c*, *Rgs4*, *Myh8*, *Ndst4*, and *Hjurp*; are also co-regulated by *Dbx1* and *Tcf7l2*. *Mef2c* is expressed in multiple brain regions including the cerebral cortex, midbrain, and cerebellum, and is crucial for neuronal differentiation, synaptic activity, learning, and memory [77]. However, the functional roles of these target genes in the midbrain remain unexplored. It should be noted that this *Dbx1*-regulated transcriptional program is not likely to be mediated entirely by the action of the *Tcf7l2-Ap-2δ* cascade. For example, *Meis2*, which marks most IC cells along with *Tcf7l2*, is regulated by *Dbx1*, but not by *Tcf7l2*. Previous gain-of-function experiments performed in chicken embryos demonstrated the ability of *Meis2* to cause a diencephalic-to-tectal fate change without inducing the isthmic organizer [24]. The question of whether a parallel action by other transcription factors participates in the regulation of IC development by *Dbx1* needs further investigation.

A remarkable feature common to *Dbx1*, *Tcf7l2* and *Ap-2δ* mutants is abnormal cell death in the posterior tectum that commences at a late developmental phase and leads postnatally to specific loss of the IC. Considering the known roles and temporal expression window of *Dbx1*, we anticipated that *Dbx1* function in the midbrain may be restricted to early embryonic patterning events. However, we discovered a novel function of *Dbx1* as a survival factor that can transcriptionally suppress the pro-apoptotic factors *c-Jun*, *Bim* and *Hrk*. The apoptotic functions of c-Jun and BH3-only proteins are limited by multiple mechanisms (transcriptional, post-transcriptional, and post-translational), and stimuli by death signals release these controls [78]. Apoptotic stimuli induce transcriptional upregulation of *c-Jun*, *Bim* and *Hrk*, causing neuronal cell death [65, 68, 79]. We show that like the loss of *Dbx1*, the loss of *Tcf7l2* also results in ectopic induction of *c-Jun*, *Bim* and *Hrk*. During embryonic development, Wnt signaling facilitates or inhibits apoptosis depending on the cellular context [48, 80]. Loss of *Wnt1* leads to the absence of midbrain and cerebellum due to increased apoptotic cell death at E9.5 [10, 18], and *β-catenin*-deficient mice exhibit pronounced apoptosis at E7.5 [81]. Unlike loss of *Wnt1* or *β-catenin*, loss of *Tcf7l2* resulted in abnormal cell death in the IC at ~E18.5. At early stages, all four *Tcf/Lef* factors are expressed in the midbrain, but at late embryonic and postnatal stages, only *Tcf7*l2 expression is strongly present in the IC (Allen Brain Atlas). Therefore, it is likely that other *Tcf/Lef* factors may compensate for the loss of *Tcf7l2* in the early stages, but not at later stages, when *Tcf7l2* is the only gene expressed in the IC. Like in *Dbx1* and *Tcf7l2* mutants, at the early stages, apoptosis does not occur in *Ap-2δ* mutants, although *Ap-2δ* is already expressed [57]. Interestingly, *Ap-2* genes are expressed in the developing midbrain in a pattern similar to that of *Tcf/Lef* factors. Five *AP-2* genes are expressed in the developing midbrain, but only *Ap-2δ* expression continues in the IC during the late embryonic and adult stages [57] (Allen Brain Atlas), suggesting that functional redundancy may exist or that early midbrain development may not be dependent on *Ap-2δ* [57, 74, 75]. As *Tcf7l2* and *Ap-2δ* are positively regulated by *Dbx1*, we assessed the ability of *Tcf7l2* and *Ap-2δ* to rescue apoptosis induced by *Dbx1* deficiency. We found that these two factors were able to decrease apoptosis and increase survival of *Dbx1*-deficient IC cells. These observations suggest that *Tcf7l2* and *Ap-2δ* are required for *Dbx1*-mediated IC survival. However, individual or combined expression of these factors showed incomplete rescue, suggesting that the ability of *Dbx1* to promote IC survival is not likely to be mediated entirely by the anti-apoptotic function of *Tcf7l2* and *Ap-2δ* . Among the IC-enriched genes regulated by *Dbx1*, but not by *Tcf7l2*, *Meis2* has been shown to prevent neuronal apoptosis [82]. Yang et al. generated *Meis2* conditional mutant mice by using *Dlx5/6-Cre* to inactivate *Meis2* in the ventral telencephalon. Loss of *Meis2* resulted in significantly increased apoptotic cell death in the developing striatum, and altered transcription factor networks involved in regulating neuronal apoptosis [82]. Whether *Meis2* participates in the regulation of IC survival requires further investigation.

MATERIALS AND METHODS

Mouse lines

All animal procedures were carried out in accordance with the guidelines and protocols approved by the Kyung Hee University Institutional Animal Care and Use Committee. The generation of *Dbx1*$^{loxp/loxp}$, *Tcf7l2*$^{loxp/loxp}$, *ROSA-Tomato* and *EIIa-Cre* mice obtained from The Jackson Laboratory, Bar Harbor, ME. was described previously [44, 58, 70, 83]. All animals used for these experiments were maintained on mixed backgrounds.

Production of transgenic mice

The *Sre* sequence was amplified by PCR with the primers (5′-ATTAG CGGCCGCAT TGCCATGGCAACGACTGCTC-3′; 5′-ATTAGCGGCCGCGGTCCAT TTTGAGGTA AATTACAGG), and cloned into the *NotI* site of an expression vector containing a β-globin minimal promoter, the *Cre* gene, and an SV40 poly(A) signal. The resulting plasmid transgene was prepared and linearized with *Sal*I for microinjection as previously described [69]. Transient transgenic embryos or mouse lines were generated by pronuclear injection into fertilized eggs derived from the FVBN mouse strain.

Immunohistochemistry

For immunohistochemistry, embryos fixed in 4% formaldehyde for 2–3 h at 4 °C were immersed in 30% sucrose, and cryosectioned at 25 µm. The following primary antibodies were used: anti-Caspase3 (Cell Signaling, 9661; 1:1000), anti-phospho-Histone H3 (Upstate Biotechnology, 06–570; 1:1000), anti-GFP (Abcam ab6673, 1:500), anti-Tcf7l2 (Millipore, 05–511, 1:200), anti-Tdtomato (SICGEN, AB8181–200, 1:500), and anti-Nrgn (Millipore, AB5620, 1:500). Following incubation with primary antibody, sections were incubated with species-specific secondary antibodies conjugated to Alexa Fluor (Molecular Probes, A11034, A11003, A11010, A11029, A11055, A11056; 1:200).

Whole-mount and section in situ hybridization

Whole-mount and section in situ hybridization were performed using digoxigenin-UTP-labeled riboprobes essentially as described previously [54]. The pairs of PCR primer sequences to generate template DNA for in vitro transcription by T7 RNA polymerase were obtained from the Allen Brain Atlas or designed against unique regions of transcripts to avoid cross-reactivity. At least three independent experiments were performed for any given riboprobes, which showed highly reproducible gene expression data.

Real-time RT-PCR

After IC tissues were harvested in TRIzol Reagent (Invitrogen), total RNA was isolated using an RNeasy Mini kit (Qiagen) and used to prepare cDNA

using a SuperScriptIII first-strand synthesis system (Invitrogen). Real-time PCR was performed in duplicates for each RNA sample using QuantiTect SYBR Green Supermix (Qiagen) following the manufacturers' instructions. Reactions were monitored using the Mx4000 multiplex quantitative PCR system (Stratagene, La Jolla, CA). All results were normalized to the housekeeping gene β-actin and relative quantification was calculated using comparative threshold cycle values for three biological replicates.

RNA-seq analysis

E18.5 IC regions were dissected, and RNA was extracted using the TRIzol Plus RNA Purification Kit (Invitrogen). Triplicates of nine IC tissues for each genotypes were run for RNA-seq (Table S1). After adaptor sequences and low-quality reads were filtered out, the clean reads from each sample were aligned to the mouse genome mm10 assembly from the University of California, Santa Cruz (UCSC), and tag counts were performed with Bowtie2 using HISAT2 (Table S1). After normalization of the read counts, transcript levels were calculated and presented by FPKM and TPM. Genes with $\log_2(FC) \geq 0.4$ and $\log_2(FC) \leq -0.4$ and FDR adjusted P value (q-value) ≤ 0.05 were considered to be differentially expressed. After statistical tests, we performed functional annotation and GO term assignment with the g:Profiler tool (https://biit.cs.ut.ee/gprofiler/), Panther (http://www.pantherdb.org) and KEGG database (http://www.genome.jp/kegg/). GO term enrichments were tested with Fisher's exact test, and FDR-adjusted P values (q-value) ≤ 0.01 were considered significant.

Primary cell culture and transfection

Brain tissues were isolated from individual embryos at E15.5 and dissected in 3 cm sterile Petridish containing ice cold dissection medium, consisting of Hanks' balanced salt solution (HBSS) (Gibco), 20 mM D-glucose (Sigma), 100 units/ml Penicillin/Streptomycin (Gibco), and 200 µM ascorbic acid (Sigma). IC tissues were collected in a 1.5 ml sterile tube and digested with StemPro Accutase Cell Dissociation reagent (Thermo Fisher Scientific) for 10–20 min at 37 °C. The digestion was stopped by removing the supernatant and washing the tissue with dissociation medium, consisting of Neurobasal medium (Invitrogen), 200 µM L-glutamine (Thermo Fisher Scientific), 2% B-27 supplement (Thermo Fisher Scientific), 2% B-27 supplement Plus (Thermo Fisher Scientific), 1% FBS (Gibco), and 200 µM ascorbic acid. The tissue was resuspended in 1 ml dissociation medium and triturated to achieve single cell suspension. After cells were spun at $200 \times g$, the cell pellet was resuspended in the dissociation medium. For immunofluorescence microscopy, the cell suspension was transferred on top of 12 mm coverslips coated with 20 µg/ml poly-L-ornithine (Sigma) and 10 µg/ml laminin (Thermo Fisher Scientific) (100,000 cells per coverslip). After 1 h incubation in a humidified tissue culture incubator at 37 °C at 5% CO_2, the coverslips were carefully transferred into 24-well plates containing the dissociation medium. Transient transfection was performed at 3 days in vitro. Transfected plasmids (0.3 µg) consisted of a mixture of 0.1 µg *CAG-NLS-GFP* [84] (a gift from Viviana Gradinaru; Addgene plasmid # 104061) + 0.2 µg *p043-mTcf4B* [85] (a gift from Ramesh Shivdasani; Addgene plasmid # 11031); a mixture of 0.1 µg *CAG-NLS-GFP* + 0.2 µg *pCMV6-Tfap2d* (Origene); a mixture of 0.1 µg *CAG-NLS-GFP* + 0.1 µg *p043-mTcf4* + 0.1 µg *pCMV6-Tfap2d*. Mock transfection consisted of 0.1 µg *CAG-NLS-GFP* + 0.2 µg empty vector. For individual wells in 24-well plates, a total of 0.3 µg DNA was diluted in 25 µl Opti-MEM Reduced Serum Medium (Gibco), and 2.5 µl Lipofectamine 2000 (Invitrogen) was diluted in 25 µl Opti-MEM in a separate tube. The diluted DNA-lipofectamine mixture was incubated at RT for 20 min and applied to cells.

Cell viability

The viability of cells in culture was assessed by measuring the activity of intracellular esterase using a Live Cell Imaging kit (Invitrogen). The non-fluorescent acetomethoxy derivative of calcein (calcein AM) is a cell permeable dye that can be transported into live cells. In living cells, calcein AM is converted to fluorescent calcein after hydrolysis by esterase. As dead cells lack active esterase, only live cells are labeled. IC-derived cells were plated on poly-L-ornithine and laminin coated coverslips in 24-well plates and allowed to culture for 1–4 weeks. After Calcein AM was added to the cells and incubated for 15 min, six randomly chosen fields from each coverslip were photographed, and the number of surviving cells was computed.

Statistical analysis

All mutant phenotypes we report in *Dbx1*^{del}, *Dbx1*^{cko}, *Tcf7l2*^{del}, and *Tcf7l2*^{cko} mice were completely penetrant in both embryos and postnatal animals. The number of independent values in each experiment was as follows: Fig. 1, three independent biological replicates for RNA-seq. Each replicate was prepared from nine IC tissues of E18.5 control and *Dbx1*^{del}. $n = 3$ for E18.5 ISH; Fig. 2, $n = 3$ for real-time RT-PCR, $n = 3$ for E18.5 ISH, $n = 5$ for E12.5-E18.5 Caspase3 staining; Fig. 3, $n = 3$ for P3 ISH, $n = 5$ for P3 Caspase3 staining, $n = 5$ for P20 ISH; Fig. 4, three independent biological replicates for RNA-seq. Each replicate was prepared from nine IC tissues of E18.5 control and *Tcf7l2*^{del}. $n = 3$ for E18.5 ISH; Fig. 5, $n = 3$ for real-time RT-PCR, $n = 3$ for E18.5 ISH, $n = 5$ for Caspase3 and PH3 immunohistochemistry; $n = 5$ for P20 ISH; Fig. 6, $n = 3$ for real-time RT-PCR, $n = 3$ for ISH; Fig. 7, $n = 5$ for Caspase3 and calcein AM staining in control and *Dbx1*^{del} IC cells, $n = 4$ for Caspase3 and calcein AM staining in transfected *Dbx1*^{del} IC cells. Relevant information for each experiment including statistical tests and p values are included in the legend corresponding to each figure. In all cases, $p \leq 0.05$ is considered statistically significant and error bars represent s.e.m.

DATA AVAILABILITY

RNA-seq raw FASTQ files of wildtype and *Dbx1* mutants have been deposited into the NCBI Sequence Read Archive under bioproject ID PRJNA793387. RNA-seq raw FASTQ files of wildtype and *Tcf7l2* mutants have been deposited into the NCBI Sequence Read Archive under bioproject ID PRJNA801436.

REFERENCES

1. Winer JA, Schreiner CE. The Inferior Colliculus. New York, NY: Springer New York; 2005. https://doi.org/10.1007/b138578.
2. Oliver DL, Morest DK. The central nucleus of the inferior colliculus in the cat. J Comp Neurol. 1984;222:237–64.
3. Winer JA, Larue DT, Diehl JJ, Hefti BJ. Auditory cortical projections to the cat inferior colliculus. J Comp Neurol. 1998;400:147–74.
4. Peruzzi D, Bartlett E, Smith PH, Oliver DL. A Monosynaptic GABAergic Input from the Inferior Colliculus to the Medial Geniculate Body in Rat. J Neurosci. 1997;17:3766–77.
5. Winer JA, Saint Marie RL, Larue DT, Oliver DL. GABAergic feedforward projections from the inferior colliculus to the medial geniculate body. Proc Natl Acad Sci. 1996;93:8005–10.
6. Nakatani T, Minaki Y, Kumai M, Ono Y. Helt determines GABAergic over glutamatergic neuronal fate by repressing Ngn genes in the developing mesencephalon. Development. 2007;134:2783–93.
7. Kala K, Haugas M, Lilleväli K, Guimera J, Wurst W, Salminen M, et al. Gata2 is a tissue-specific post-mitotic selector gene for midbrain GABAergic neurons. Development. 2009;136:253–62.
8. Joyner AL, Liu A, Millet S. Otx2, Gbx2 and Fgf8 interact to position and maintain a mid-hindbrain organizer. Curr Opin Cell Biol. 2000;12:736–41.
9. Wurst W, Bally-Cuif L. Neural plate patterning: upstream and downstream of the isthmic organizer. Nat Rev Neurosci. 2001;2:99–108.
10. Chi CL, Martinez S, Wurst W, Martin GR. The isthmic organizer signal FGF8 is required for cell survival in the prospective midbrain and cerebellum. Development. 2003;130:2633–44.
11. Shamim H, Mahmood R, Logan C, Doherty P, Lumsden A, Mason I. Sequential roles for Fgf4, En1 and Fgf8 in specification and regionalisation of the midbrain. Development. 1999;126:945–59.
12. Basson MA, Echevarria D, Ahn CP, Sudarov A, Joyner AL, Mason IJ, et al. Specific regions within the embryonic midbrain and cerebellum require different levels of FGF signaling during development. Development. 2008;135:889–98.
13. Dee A, Li K, Heng X, Guo Q, Li JYH. Regulation of self-renewing neural progenitors by FGF/ERK signaling controls formation of the inferior colliculus. Development. 2016;143:3661–73.
14. Sgaier SK, Lao Z, Villanueva MP, Berenshteyn F, Stephen D, Turnbull RK, et al. Genetic subdivision of the tectum and cerebellum into functionally related regions based on differential sensitivity to engrailed proteins. Development. 2007;134:2325–35.
15. Trokovic R. FGFR1 is independently required in both developing mid- and hindbrain for sustained response to isthmic signals. EMBO J. 2003;22:1811–23.
16. Xu J, Liu Z, Ornitz DM. Temporal and spatial gradients of Fgf8 and Fgf17 regulate proliferation and differentiation of midline cerebellar structures. Development. 2000;127:1833–43.
17. Sato T, Joyner AL. The duration of Fgf8 isthmic organizer expression is key to patterning different tectal-isthmo-cerebellum structures. Development. 2009;136:3617–26.
18. McMahon AP, Bradley A. The Wnt-1 (int-1) proto-oncogene is required for development of a large region of the mouse brain. Cell. 1990;62:1073–85.

19. Thomas KR, Capecchi MR. Targeted disruption of the murine int-1 proto-oncogene resulting in severe abnormalities in midbrain and cerebellar development. Nature. 1990;346:847–50.
20. Wurst W, Auerbach AB, Joyner AL. Multiple developmental defects in Engrailed-1 mutant mice: an early mid-hindbrain deletion and patterning defects in forelimbs and sternum. Development. 1994;120:2065–75.
21. Serbedzija GN, Dickinson M, McMahon AP. Cell death in the CNS of the Wnt-1 mutant mouse. J Neurobiol. 1996;31:275–82.
22. Urbánek P, Wang ZQ, Fetka I, Wagner EF, Busslinger M. Complete block of early B cell differentiation and altered patterning of the posterior midbrain in mice lacking Pax5/BSAP. Cell. 1994;79:901–12.
23. Matsunaga E, Araki I, Nakamura H. Role of Pax3/7 in the tectum regionalization. Development. 2001;128:4069–77.
24. Agoston Z, Schulte D. Meis2 competes with the Groucho co-repressor Tle4 for binding to Otx2 and specifies tectal fate without induction of a secondary midbrain-hindbrain boundary organizer. Development. 2009;136:3311–22.
25. Broccoli V, Boncinelli E, Wurst W. The caudal limit of Otx2 expression positions the isthmic organizer. Nature. 1999;401:164–8.
26. Millet S, Campbell K, Epstein DJ, Losos K, Harris E, Joyner AL. A role for Gbx2 in repression of Otx2 and positioning the mid/hindbrain organizer. Nature. 1999;401:161–4.
27. Puelles E, Acampora D, Lacroix E, Signore M, Annino A, Tuorto F, et al. Otx dose-dependent integrated control of antero-posterior and dorso-ventral patterning of midbrain. Nat Neurosci. 2003;6:453–60.
28. Di Giovannantonio LG, Di Salvio M, Omodei D, Prakash N, Wurst W, Pierani A, et al. Otx2 cell-autonomously determines dorsal mesencephalon versus cerebellum fate independently of isthmic organizing activity. Development. 2014;141:377–88.
29. Cowan WM, Martin AH, Wenger E. Mitotic patterns in the optic tectum of the chick during normal development and after early removal of the optic vesicle. J Exp Zool. 1968;169:71–92.
30. Altman J, Bayer SA. Time of origin of neurons of the rat inferior colliculus and the relations between cytogenesis and tonotopic order in the auditory pathway. Exp Brain Res. 1981;42–42:411–23.
31. Altman J, Bayer SA. Time of origin of neurons of the rat superior colliculus in relation to other components of the visual and visuomotor pathways. Exp Brain Res. 1981;42:424–34.
32. Edwards MA, Caviness VS, Schneider GE. Development of cell and fiber lamination in the mouse superior colliculus. J Comp Neurol. 1986;248:395–409.
33. Miyoshi G, Bessho Y, Yamada S, Kageyama R. Identification of a novel basic helix-loop-helix gene, Heslike, and its role in GABAergic neurogenesis. J Neurosci. 2004;24:3672–82.
34. Guimera J, Weisenhorn DV, Wurst W. Megane/Heslike is required for normal GABAergic differentiation in the mouse superior colliculus. Development. 2006;133:3847–57.
35. Peltopuro P, Kala K, Partanen J. Distinct requirements for Ascl1 in subpopulations of midbrain GABAergic neurons. Dev Biol. 2010;343:63–70.
36. Achim K, Peltopuro P, Lahti L, Tsai HH, Zachariah A, Astrand M, et al. The role of Tal2 and Tal1 in the differentiation of midbrain GABAergic neuron precursors. Biol Open. 2013;2:990–7.
37. Wende C-Z, Zoubaa S, Blak A, Echevarria D, Martinez S, Guillemot F, et al. Hairy/Enhancer-of-Split MEGANE and Proneural MASH1 Factors Cooperate Synergistically in Midbrain GABAergic Neurogenesis. PLoS ONE. 2015;10:e0127681.
38. Shoji H, Ito T, Wakamatsu Y, Hayasaka N, Ohsaki K, Oyanagi M, et al. Regionalized expression of the Dbx family homeobox genes in the embryonic CNS of the mouse. Mech Dev. 1996;56:25–39.
39. Pierani A, Moran-Rivard L, Sunshine MJ, Littman DR, Goulding M, Jessell TM. Control of interneuron fate in the developing spinal cord by the progenitor homeodomain protein Dbx1. Neuron. 2001;29:367–84.
40. Lanuza GM, Gosgnach S, Pierani A, Jessell TM, Goulding M. Genetic identification of spinal interneurons that coordinate left-right locomotor activity necessary for walking movements. Neuron. 2004;42:375–86.
41. Talpalar AE, Bouvier J, Borgius L, Fortin G, Pierani A, Kiehn O. Dual-mode operation of neuronal networks involved in left-right alternation. Nature. 2013;500:85–8.
42. Bouvier J, Thoby-Brisson M, Renier N, Dubreuil V, Ericson J, Champagnat J, et al. Hindbrain interneurons and axon guidance signaling critical for breathing. Nat Neurosci. 2010;13:1066–74.
43. Gray PA, Hayes JA, Ling GY, Llona I, Tupal S, Picardo MC, et al. Developmental origin of preBötzinger complex respiratory neurons. J Neurosci. 2010;30:14883–95.
44. Sokolowski K, Esumi S, Hirata T, Kamal Y, Tran T, Lam A, et al. Specification of select hypothalamic circuits and innate behaviors by the embryonic patterning gene dbx1. Neuron. 2015;86:403–16.
45. Inamata Y, Shirasaki R. Dbx1 triggers crucial molecular programs required for midline crossing by midbrain commissural axons. Development. 2014;141:1260–71.
46. Grant SF, Thorleifsson G, Reynisdottir I, Benediktsson R, Manolescu A, Sainz J, et al. Variant of transcription factor 7-like 2 (TCF7L2) gene confers risk of type 2 diabetes. Nat Genet. 2006;38:320–3.
47. Korinek V, Barker N, Moerer P, van Donselaar E, Huls G, Peters PJ, et al. Depletion of epithelial stem-cell compartments in the small intestine of mice lacking Tcf-4. Nat Genet. 1998;19:379–83.
48. Li F, Chong ZZ, Maiese K. Winding through the WNT pathway during cellular development and demise. Histol Histopathol. 2006;21:103–24.
49. Ah Cho E, Dressler GR. TCF-4 binds β-catenin and is expressed in distinct regions of the embryonic brain and limbs. Mech Dev. 1998;77:9–18.
50. Brinkmeier ML, Potok MA, Davis SW, Camper SA. TCF4 deficiency expands ventral diencephalon signaling and increases induction of pituitary progenitors. Dev Biol. 2007;311:396–407.
51. Ye F, Chen Y, Hoang T, Montgomery RL, Zhao XH, Bu H, et al. HDAC1 and HDAC2 regulate oligodendrocyte differentiation by disrupting the beta-catenin-TCF interaction. Nat Neurosci. 2009;12:829–38.
52. Hammond E, Lang J, Maeda Y, Pleasure D, Angus-Hill M, Xu J, et al. The Wnt effector transcription factor 7-like 2 positively regulates oligodendrocyte differentiation in a manner independent of Wnt/β-catenin signaling. J Neurosci. 2015;35:5007–22.
53. Zhao C, Deng Y, Liu L, Yu K, Zhang L, Wang H, et al. Dual regulatory switch through interactions of Tcf7l2/Tcf4 with stage-specific partners propels oligodendroglial maturation. Nat Commun. 2016;7:10883.
54. Lee M, Yoon J, Song H, Lee B, Lam DT, Yoon J, et al. Tcf7l2 plays crucial roles in forebrain development through regulation of thalamic and habenular neuron identity and connectivity. Dev Biol. 2017;424:62–76.
55. Tran H-N, Park W, Seong S, Jeong JE, Nguyen QH, Yoon J, et al. Tcf7l2 transcription factor is required for the maintenance, but not the initial specification, of the neurotransmitter identity in the caudal thalamus. Dev Dyn. 2020;249:646–55.
56. Lipiec MA, Bem J, Koziński K, Chakraborty C, Urban-Ciećko J, Zajkowski T, et al. TCF7L2 regulates postmitotic differentiation programmes and excitability patterns in the thalamus. Development. 2020;147:dev190181.
57. Hesse K, Vaupel K, Kurt S, Buettner R, Kirfel J, Moser M. AP-2δ is a crucial transcriptional regulator of the posterior midbrain. PLoS ONE. 2011;6:e23483.
58. Lakso M, Pichel JG, Gorman JR, Sauer B, Okamoto Y, Lee E, et al. Efficient in vivo manipulation of mouse genomic sequences at the zygote stage. Proc Natl Acad Sci USA. 1996;93:5860–5.
59. Matsunaga Y, Noda M, Murakawa H, Hayashi K, Nagasaka A, Inoue S, et al. Reelin transiently promotes N-cadherin-dependent neuronal adhesion during mouse cortical development. Proc Natl Acad Sci USA. 2017;114:2048–53.
60. Chao CC-K, Chang P-Y, Lu HH-P. Human Gas7 isoforms homologous to mouse transcripts differentially induce neurite outgrowth. J Neurosci Res. 2005;81:153–62.
61. Garrido-García A, de Andrés R, Jiménez-Pompa A, Soriano P, Sanz-Fuentes D, Martínez-Blanco E, et al. Neurogranin Expression Is Regulated by Synaptic Activity and Promotes Synaptogenesis in Cultured Hippocampal Neurons. Mol Neurobiol. 2019;56:7321–37.
62. Panza P, Sitko AA, Maischein H-M, Koch I, Flötenmeyer M, Wright GJ, et al. The LRR receptor Islr2 is required for retinal axon routing at the vertebrate optic chiasm. Neural Dev. 2015;10:23.
63. Xiao T, Baier H. Lamina-specific axonal projections in the zebrafish tectum require the type IV collagen Dragnet. Nat Neurosci. 2007;10:1529–37.
64. Cooper SR, Emond MR, Duy PQ, Liebau BG, Wolman MA, Jontes JD. Protocadherins control the modular assembly of neuronal columns in the zebrafish optic tectum. J Cell Biol. 2015;211:807–14.
65. Putcha GV, Moulder KL, Golden JP, Bouillet P, Adams JA, Strasser A, et al. Induction of BIM, a proapoptotic BH3-only BCL-2 family member, is critical for neuronal apoptosis. Neuron. 2001;29:615–28.
66. Coultas L, Terzano S, Thomas T, Voss A, Reid K, Stanley EG, et al. Hrk/DP5 contributes to the apoptosis of select neuronal populations but is dispensable for haematopoietic cell apoptosis. J Cell Sci. 2007;120:2044–52.
67. Ma C, Ying C, Yuan Z, Song B, Li D, Liu Y, et al. dp5/HRK is a c-Jun target gene and required for apoptosis induced by potassium deprivation in cerebellar granule neurons. J Biol Chem. 2007;282:30901–9.
68. Whitfield J, Neame SJ, Paquet L, Bernard O, Ham J. Dominant-Negative c-Jun Promotes Neuronal Survival by Reducing BIM Expression and Inhibiting Mitochondrial Cytochrome c Release. Neuron. 2001;29:629–43.
69. Lee B, Song H, Rizzoti K, Son Y, Yoon J, Baek K, et al. Genomic code for Sox2 binding uncovers its regulatory role in Six3 activation in the forebrain. Dev Biol. 2013;381:491–501.
70. Angus-Hill ML, Elbert KM, Hidalgo J, Capecchi MR. T-cell factor 4 functions as a tumor suppressor whose disruption modulates colon cell proliferation and tumorigenesis. Proc Natl Acad Sci. 2011;108:4914–9.

71. Schorle H, Meier P, Buchert M, Jaenisch R, Mitchell PJ. Transcription factor AP-2 essential for cranial closure and craniofacial development. Nature. 1996;381: 235–8.
72. Moser M, Pscherer A, Roth C, Becker J, Mücher G, Zerres K, et al. Enhanced apoptotic cell death of renal epithelial cells in mice lacking transcription factor AP-2beta. Genes Dev. 1997;11:1938–48.
73. Malmierca MS, Blackstad TW, Osen KK, Karagülle T, Molowny RL. The central nucleus of the inferior colliculus in rat: A Golgi and computer reconstruction study of neuronal and laminar structure. J Comp Neurol. 1993;333:1–27.
74. Meininger V, Pol D, Derer P. The inferior colliculus of the mouse. A Nissl and Golgi study. Neuroscience. 1986;17:1159–79.
75. Chen C, Cheng M, Ito T, Song S. Neuronal Organization in the Inferior Colliculus Revisited with Cell-Type-Dependent Monosynaptic Tracing. J Neurosci. 2018;38: 3318–32.
76. Goyer D, Silveira MA, George AP, Beebe NL, Edelbrock RM, Malinski PT, et al. A novel class of inferior colliculus principal neurons labeled in vasoactive intestinal peptide-Cre mice. Elife. 2019;8:e43770.
77. Li H, Radford JC, Ragusa MJ, Shea KL, McKercher SR, Zaremba JD, et al. Transcription factor MEF2C influences neural stem/progenitor cell differentiation and maturation in vivo. Proc Natl Acad Sci USA. 2008;105:9397–402.
78. Fricker M, Tolkovsky AM, Borutaite V, Coleman M, Brown GC. Neuronal Cell Death. Physiol Rev. 2018;98:813–80.
79. Imaizumi K. Critical Role for DP5/Harakiri, a Bcl-2 Homology Domain 3-Only Bcl-2 Family Member, in Axotomy-Induced Neuronal Cell Death. J Neurosci. 2004;24: 3721–5.
80. Ellies DL, Church V, Francis-West P, Lumsden A. The WNT antagonist cSFRP2 modulates programmed cell death in the developing hindbrain. Development. 2000;127:5285–95.
81. Huelsken J, Vogel R, Brinkmann V, Erdmann B, Birchmeier C, Birchmeier W. Requirement for beta-catenin in anterior-posterior axis formation in mice. J Cell Biol. 2000;148:567–78.
82. Yang L, Su Z, Wang Z, Li Z, Shang Z, Du H, et al. Transcriptional profiling reveals the transcription factor networks regulating the survival of striatal neurons. Cell Death Dis. 2021;12:262.
83. Madisen L, Zwingman TA, Sunkin SM, Oh SW, Zariwala HA, Gu H, et al. A robust and high-throughput Cre reporting and characterization system for the whole mouse brain. Nat Neurosci. 2010;13:133–40.
84. Challis RC, Ravindra Kumar S, Chan KY, Challis C, Beadle K, Jang MJ, et al. Systemic AAV vectors for widespread and targeted gene delivery in rodents. Nat Protoc. 2019;14:379–414.
85. Lee YJ, Swencki B, Shoichet S, Shivdasani RA. A possible role for the high mobility group box transcription factor Tcf-4 in vertebrate gut epithelial cell differentiation. J Biol Chem. 1999;274:1566–72.

ACKNOWLEDGEMENTS

This work was supported by the National Research Foundation of Korea (NRF) grants funded by the Korea Ministry of Science and ICT (No. 2019R1F1A1042941 and No. 2022R1F1A1064555).

AUTHOR CONTRIBUTIONS

Conceived project: YJ. Designed experiments: HT, YJ. Performed experiments: HT, QN, JJ, DL. Analyzed data: HT, QN, JJ, DL, YJ. Provided reagents: YN, TK, JY, KB, Wrote paper: YJ. Reviewed and revised the paper: HT, QN, JJ, DL, YJ.

COMPETING INTERESTS

The authors declare no competing interests.

ETHICS APPROVAL

All animal experiments were conducted in accordance with the guidelines of the Kyung Hee University Institutional Animal Care and Use Committee (KHGASP-20–015).

ADDITIONAL INFORMATION

Supplementary information The online version contains supplementary material available at https://doi.org/10.1038/s41418-023-01165-6.

Correspondence and requests for materials should be addressed to Yongsu Jeong.

Reprints and permission information is available at http://www.nature.com/reprints

Publisher's note Springer Nature remains neutral with regard to jurisdictional claims in published maps and institutional affiliations.